Blocking and General Circulation in GFDL Comprehensive Climate Models

Veeshan Narinesingh,[a,b,c] James F. Booth,[a,b,c] and Yi Ming[d]

[a] *Department of Physics, Graduate Center, City University of New York, New York, New York*
[b] *Department of Earth and Atmospheric Sciences, City College, City University of New York, New York, New York*
[c] *NOAA-CESSRST, City College, City University of New York, New York, New York*
[d] *Geophysical Fluid Dynamics Laboratory/NOAA, Princeton, New Jersey*

ABSTRACT: This study examines the climatology and dynamics of atmospheric blocking, and the general circulation features that influence blocks in GFDL's atmosphere-only (AM4) and coupled atmosphere–ocean (CM4) comprehensive models. We compare AM4 and CM4 with reanalysis, focusing on winter in the Northern Hemisphere. Both models generate the correct blocking climatology and planetary-scale signatures of the stationary wave. However, at regional scales some biases exist. In the eastern Pacific and over western North America, both models generate excessive blocking frequency and too strong of a stationary wave. In the Atlantic, the models generate too little blocking and a weakened stationary wave. A block-centered compositing analysis of block-onset dynamics reveals that the models 1) produce realistic patterns of high-frequency (1–6-day) eddy forcing and 2) capture the notable differences in the 500-hPa geopotential height field between Pacific and Atlantic blocking. However, the models fail to reproduce stronger wave activity flux convergence in the Atlantic compared to the Pacific. Overall, biases in the blocking climatology in terms of location, frequency, duration, and area are quite similar between AM4 and CM4 despite the models having large differences in sea surface temperatures and climatological zonal circulation. This could suggest that other factors could be more dominant in generating blocking biases for these GCMs.

SIGNIFICANCE STATEMENT: Atmospheric blocks are persistent high pressure systems that can lead to hazardous weather. Historically, climate models have had trouble capturing blocks, but recent changes in the models might lead to improvements. As such, the work herein investigates the spatial distribution, prevalence, duration, size, and dynamics of wintertime blocking in recent NOAA climate models. Overall, these models capture the long-term-average spatial pattern of blocking, and properly reproduce key dynamical features. However, the models produce too much blocking in the western United States, and too little over the northern Atlantic Ocean and Europe. These blocking biases are consistent with atmospheric stationary waves biases, but not jet stream bias. This downplays the role of jet biases in the models being responsible for blocking biases.

KEYWORDS: Anticyclones; Blocking; Eddies; Planetary waves; Stationary waves; Climate models; Coupled models; General circulation models; Reanalysis data

---

1. Introduction

Atmospheric blocks are persistent, quasi-stationary anticyclones (Rex 1950) that can impact midlatitude weather hazards (Sillmann 2011; Pfahl and Wernli 2012; Booth et al. 2021), cyclonic weather systems (Mattingly et al. 2015; Yamazaki et al. 2015; Booth et al. 2017), and climate [reviewed in Lupo (2020)]. As such, it is important to understand how blocking will respond to anthropogenic climate change (e.g., Woollings et al. 2018). However, we first need to understand and quantify the skill of the most recent generation of general circulation models (GCMs) in capturing blocking in current climates and determine how the representation of blocking depends on model general circulation features. Therefore, the work herein analyzes the climatological and dynamical features of blocking in integrations of GFDL's atmosphere-only and coupled atmosphere–ocean comprehensive

models for the recent past (i.e., historical integrations from the model intercomparison projects).

Past assessments of GCMs show that the models have issues in capturing blocking. For instance, D'Andrea et al. (1998) analyzed how well the climatological features of blocking were captured in the first Atmospheric Model Intercomparison Project (AMIP). They found that all 15 models underestimated blocking in both the Pacific and Atlantic regions. Since then, various studies have assessed the climatology of blocking across different generations of coupled models that participated in Coupled Model Intercomparison Project (CMIP) experiments (Scaife et al. 2011; Barnes et al. 2012; Masato et al. 2013; Anstey et al. 2013; Davini and D'Andrea 2020). In all cases modeled blocking climatology did not quantitatively match reanalysis. Furthermore, biases in blocking have been found to vary greatly across models, with the Pacific and Atlantic sometimes showing opposite signs in biases (Matsueda et al. 2009; Masato et al. 2013; Jiang et al. 2019).

In the multimodel mean of the CMIP6 models, blocking across the Northern Hemisphere is biased low in terms of blocking frequency (Davini and D'Andrea 2020; Schiemann et al. 2020). These biases have been attributed to mean-state biases (Scaife et al. 2011; Davini and D'Andrea 2016; Kleiner et al. 2021).
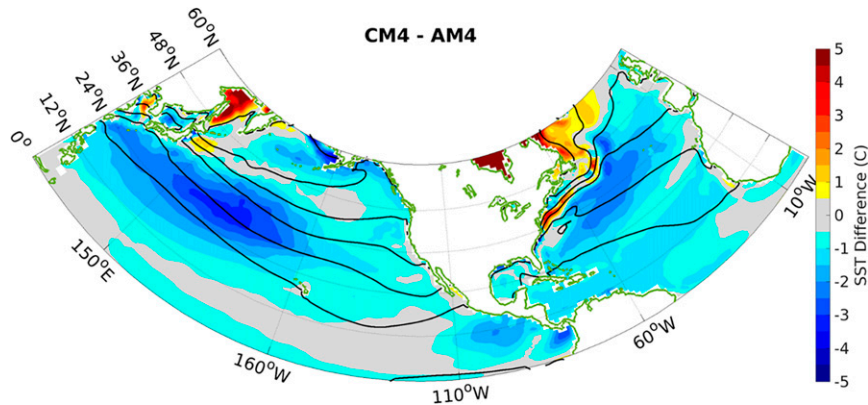
FIG. 1. Sea surface temperature (SST) in AM4 (contours) and difference in SST between CM4 and AM4 (shading). The most equatorward contour is 30°C, and the contour interval is 5°C.

Other more targeted studies, however, suggest that subgrid-scale processes that would likely be more accurately represented by increasing horizontal resolution could be causing biases in a model's representation of blocking (Jung et al. 2012; Anstey et al. 2013; Davini et al. 2017; Jiang et al. 2019; Steinfeld et al. 2020). Thus, the current state of the literature suggests that both the large-scale and small-scale dynamical features of GCMs might explain model blocking biases.

Theoretical work on blocking offers additional motivation as one considers potential mechanisms for model biases. The recent idealized modeling work of Paradise et al. (2019) suggests that the dynamical details of the models could have important impacts on the blocking climatology. The authors systematically analyze the stationary wave, jet, and high-frequency eddy feedback using the "traffic jam" theory introduced by Nakamura and Huang (2018). Paradise et al. (2019) found that the stationary wave and high-frequency eddy forcing exhibited a direct relationship with blocking, whereas stronger jets led to less blocking.

Other authors have found the position of the jet, and thus waveguide, to be key to blocking. In work with early models and observations, Yeh (1949) found blocking to be more persistent for higher jet latitudes. Recently, Wang and Kuang (2019) expanded upon the idealized modeling work of Shutts (1983) to show that the orientation of high-frequency eddies, not their presence alone, plays a pivotal role in maintaining blocks, yielding results in agreement with Yeh (1949) in terms of jet latitude, eddy orientation, and blocking. Using comprehensive models, however, Barnes and Hartmann (2010) found a decrease in blocking for higher jet latitudes. Clearly, a full theory of blocking frequency and its relationship to the mean state is not yet settled. These studies provide context and motivation for more detailed analysis of the links between large-scale features of GCM atmospheric dynamics and modeled blocking.

With this in mind, the study herein investigates the climatology and dynamics of blocking in version 4 of GFDL's atmosphere-only and coupled atmosphere–ocean models (AM4 and CM4). The remainder of the paper is organized as follows: section 2 covers the data and methods. In section 3a, we analyze model simulation of the stationary wave and upper-level jet.

In section 3b, we evaluate the blocking climatology. In section 3c, block area and duration in the GFDL models is compared to reanalysis. The background flow and transient eddy forcing during block onset is investigated in sections 3d and 3e, respectively; for this, block-centered compositing analyses of geopotential height, low-frequency zonal wind, and high-frequency eddy forcing are separately carried out for Pacific and Atlantic blocking. Section 4 provides a discussion of consistencies and inconsistencies in general circulation and blocking biases in the models. Section 5 presents conclusions.

2. Data and methods

a. General circulation models

This work analyzes general circulation and blocking in Geophysical Fluid Dynamics Laboratory's (GFDL) atmosphere-only model AM4 (Zhao et al. 2018) and coupled atmosphere–ocean model CM4 (Held et al. 2019). Previous studies have shown strong agreement between GFDL blocking simulations and corresponding CMIP ensemble means (Masato et al. 2013; Davini and D'Andrea 2016). AM4 is computed at roughly 100-km resolution with 33 vertical levels. AM4 is forced with prescribed time-evolving sea surface temperatures (SSTs) and sea ice distributions. AM4 serves as the atmospheric component for the coupled model CM4, which is part of the ensemble from phase 6 of the Coupled Model Intercomparison Project (CMIP6). CM4 consists of AM4 coupled to the ocean model, OM4 (Adcroft et al. 2019), and sea ice model SIS2.0 (Adcroft et al. 2019). The CM4 simulation is not retuned relative to the AM4 simulation with prescribed forcing.

The primary difference between AM4 and CM4 is ocean forcing. AM4 is forced by prescribed SSTs while CM4 is coupled to an ocean model. Generally, the mean SSTs in CM4 are colder than AM4 during winter (December–February; Fig. 1). These biases have been documented in Held et al. (2019; see their Fig. 13); for the most part, they are smaller than biases in previous GFDL models. CM4 is also coupled to a dynamic sea ice model, whereas the sea ice in AM4 is a time-evolving parameterization based on observations. CM4 also uses a different land model,
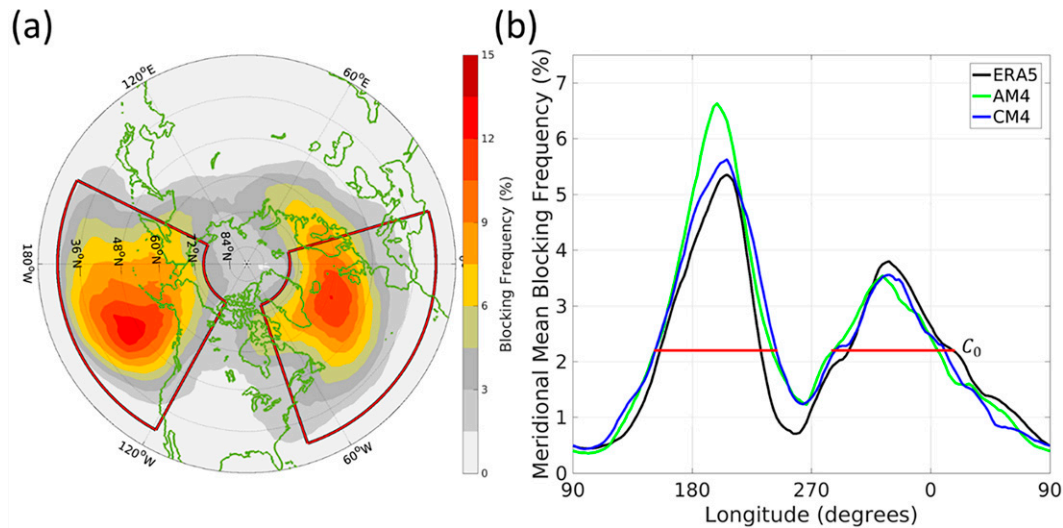
FIG. 2. (a) Blocking climatology C (shading) for ERA5 averaged over December–February (DJF). Red boxes show the boundaries used to define the Pacific and Atlantic regions. (b) Area-weighted meridional mean of the midlatitude DJF blocking climatology $\tilde{C}$ in ERA5, AM4, and CM4. The horizontal red lines denote the Pacific and Atlantic regions. C_0 is the minimum blocking frequency used to define each region.

LM4.0.01, compared to AM4, which uses LM4.0. The version LM4.0.01 contains different settings controlling albedos of snow masking involving vegetation and glaciers. More information on this can be found in Held et al. (2019).

The jet at 250 hPa, stationary wave at 500 hPa, and blocking produced by the GFDL models are compared with ECMWF ERA5 reanalysis (Hersbach et al. 2020). ERA5 is produced at roughly 30-km horizontal resolution with 137 vertical levels. For all models in this paper, daily mean data are interpolated into $2.0°$ latitude $\times$ $2.5°$ longitude grids. We focus only on winter defined as December–February (DJF) from 1980 to 2014.

b. Block tracking, climatology, and regional sorting

To identify and track blocks, this work implements the 500-hPa geopotential height (Z_{500}) metric described by Dunn-Sigouin and Son (2013, herein DS13). This hybrid metric searches for strong positive anomalies in Z_{500} (Z'_{500}) that reverse the meridional gradient of Z_{500}. The anomalies are calculated at each point in space by removing a running annual mean and mean seasonal cycle, similar to a 30-day high-pass filter. To identify blocking candidates, the tracking algorithm implements several thresholds on contiguous Z'_{500} anomalies:

1) Positive anomaly amplitude of at least 1.5 standard deviations
2) Area of at least 2.5×10^6 km^2
3) Meridional gradient reversal of Z_{500} as described in DS13
4) Quasi-stationary condition: 50% area overlap between successive time steps
5) Satisfaction of the above criteria for at least 5 days

We choose this metric due to its straightforward implementation, as well as its ability to capture high-amplitude wave breaking events (DS13). Barnes et al. (2012) found that similar Z_{500} metrics yield similar blocking properties

and climatological features compared to potential temperature or vorticity-based metrics. For specific details of the tracking algorithm, the reader is referred to DS13.

For each time step at each grid point, the block tracker yields a block identification flag of 1 or 0 corresponding to the presence and absence, respectively, of blocking. Climatological spatial distributions of blocking frequency, hereinafter referred to as the blocking climatology, are computed by averaging 2D latitude–longitude grids of block identification flags over all DJF days. Note that, in this work, blocking frequency indicates the percentage of DJF time steps that a grid point was identified as blocked, not the number of individual events. The blocking climatology for DJF in ERA5 from 1980–2014 is shown in Fig. 2a.

Previous studies have found distinct differences between Pacific and Atlantic blocking in the Northern Hemisphere (Hartmann and Ghan 1980; Nakamura et al. 1997). Furthermore, within general circulation models, blocking simulation biases in the Pacific and Atlantic are often in disagreement in terms of sign and magnitude (Matsueda et al. 2009; Masato et al. 2013). Thus, for this study, blocking is sorted into two major regions of study: the Pacific region, and the Atlantic region. These regions are indicated by the red boxes in Fig. 2a.

The spatial extent of these regions is determined as follows. The DJF blocking climatology C for ERA5, AM4, and CM4 is separately calculated. Next, the area-weighted meridional-mean of C, $\tilde{C}$, is calculated between $30°$ and $75°$N for reanalysis and for each GFDL model (Fig. 2b); For this, the southern boundary of $30°$N is set by the tracking algorithm and the northern limit is chosen to exclude polar blocking [see Berrisford et al. (2007) for more discussion on polar blocking]. The term $[\tilde{C}]$ is the zonal mean of $\tilde{C}$, and it represents the area-weighted blocking frequency within the midlatitudes of each model. For ERA5, AM4, and CM4, $[\tilde{C}]$ is equal to 2.0%, 2.17%, and 2.16%, respectively.
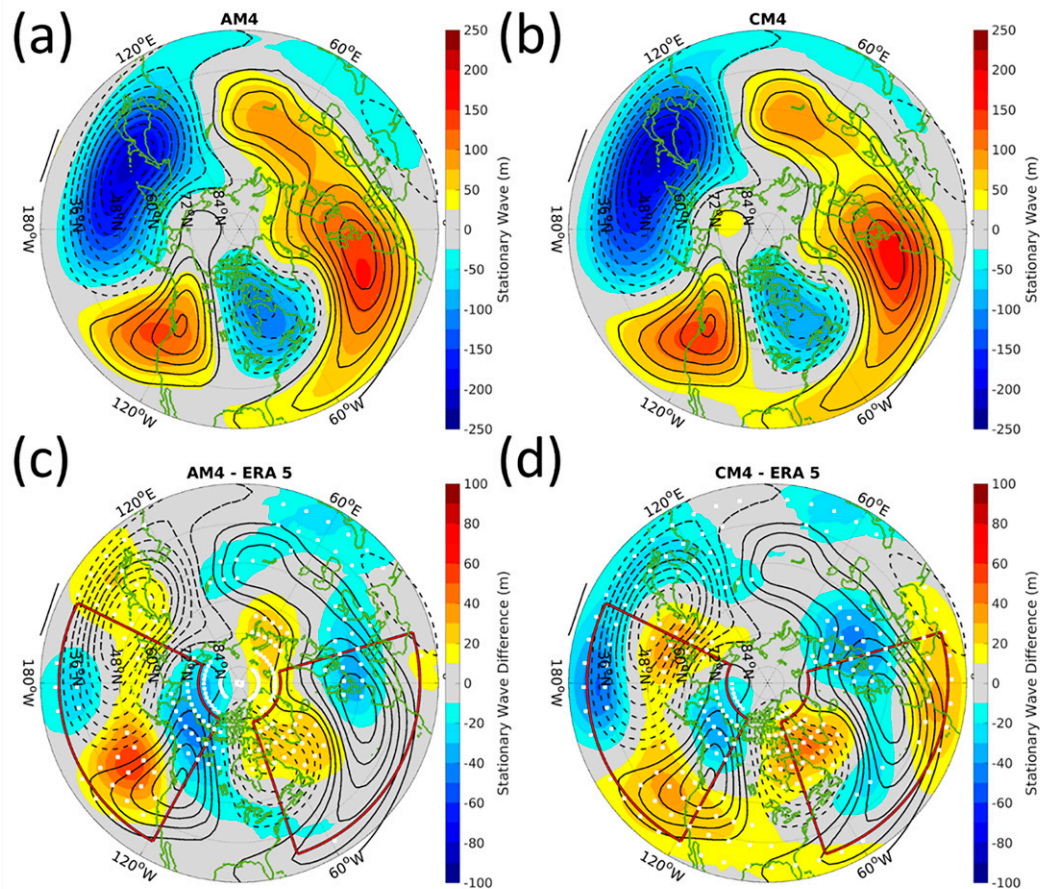
FIG. 3. (top) DJF stationary wave at 500 hPa (Z_{500}^*) for ERA5 (contours) and the GFDL models (shading): (a) AM4 and (b) CM4. (bottom) Z_{500}^* for ERA5 (contours) and Z_{500}^* in the GFDL models minus reanalysis (shading) for (c) AM4 and (d) CM4. Solid and dashed contours in all panels show the positive and negative Z_{500}^*, respectively. The outer contour for the solid (dashed) contours is 25 (-25) m and the contour interval is 25 (-25) m. White stippling in (c) and (d) denotes regions where Z_{500}^* in the GFDL models differ significantly from ERA5.

Figure 2b shows two distinct peaks in $\tilde{C}$ where blocking is most ubiquitous. These correspond to the Pacific and Atlantic blocking maxima in Fig. 2a. To define the Atlantic and Pacific regions, peaks in $\tilde{C}$ with values above a threshold C_0 are identified in each model, where C_0 is defined as the minimum of $[\tilde{C}]$ across all models and equals 2.0%. The eastern and western limits of each region are defined as the longitudes at which any model exceeds C_0 (the horizontal line in Fig. 2b). This is done to capture the greatest area and account for any zonal shifts in blocking. Based on this methodology, the Pacific and Atlantic regions span 153.75°E–118.75°W and 71.25°W–16.25°E, respectively.

In our analysis of block duration, we have to account for the fact that some blocks move out of the study region during their individual life cycles. To avoid miscounting, we classify the blocks based on their origin, and we keep track of their life cycles based on their time within the study regions as follows. A block is classified as originating in the Pacific or Atlantic if the location of its Z'_{500} maximum falls within the respective region during the block's first time step. Block area is defined as the contiguous area of blocked pixels—even if some of the block is located outside of the study region. For Pacific and Atlantic classified blocks, regional block duration is defined as continuous time steps from the onset of the block until the block area has less than 50% of the tracking algorithm's area threshold (2.6×10^6 km²) within the region. Block area, duration, and compositing results are robust to changes $\pm 10°$ to the region boundaries.

c. Stationary wave and mean zonal wind

Two blocking-relevant general circulation features are examined within this paper: the stationary wave and zonal wind. Results presented in this paper for the stationary wave and the zonal wind were not strongly impacted by the inclusion or removal of blocked grid points in each respective calculation.

The stationary wave is calculated on the Z_{500} field. The stationary wave at each grid point Z_{500}^* is defined using the equation $Z_{500}^* = \overline{Z_{500}} - [\overline{Z_{500}}]$. Here, overbars indicate the DJF time mean, and brackets indicate the zonal mean. The time

mean of the 250-hPa zonal wind is referred to as $\overline{U_{250}}$. This is the DJF climatology of the upper-level jet. We also analyze the zonal mean of the zonal wind climatology: $[\overline{U}]$.

d. Transient eddy forcing: Wave activity flux

The wave activity flux **W** (Takaya and Nakamura 2001, herein TN01) can be described as the "ageostrophic flux of geopotential" and represents the pseudomomentum of Rossby waves. Convergent **W** indicates the halted propagation and absorption of Rossby waves (TN01). The **W** convergence is associated with decreased zonal flow, the amplification of Rossby waves, and accompanies wavebreaking (Nakamura et al. 1997; TN01; Wolf and Wirth 2017), reinforcing blocked flows (TN01).

The wave activity flux **W** is defined as follows:

$$\mathbf{W} = \frac{p\cos\phi}{2|\mathbf{U}|}\begin{Bmatrix} U\left(v'^2 - \dfrac{\Phi'}{f}\dfrac{\partial v'}{\partial x}\right) + V\left(-u'v' - \dfrac{\Phi'}{f}\dfrac{\partial v'}{\partial y}\right) \\ U\left(-u'v' + \dfrac{\Phi'}{f}\dfrac{\partial u'}{\partial x}\right) + V\left(u'^2 + \dfrac{\Phi'}{f}\dfrac{\partial u'}{\partial y}\right) \end{Bmatrix}. \quad (1)$$

At a given pressure level, u', v', and Φ' are the 6-day high-pass filtered zonal wind, meridional wind, and geopotential, respectively. The background flow, **U**, contains 30-day low-pass-filtered zonal wind, U, and meridional wind, V. Pressure is denoted by p, f is the Coriolis parameter, and ϕ is latitude. This quantity is computed at five pressure levels between 950 and 250 hPa and then the mass-weighted vertical integral is performed for the block-centered compositing analyses in this paper.

We note that the phase propagation term in the TN01 formulation is omitted in our analysis. This is due to difficulties in accurately calculating phase speed on all pressure levels for each model. However, in a comparison with the results of Wolf and Wirth (2017), the stationary term was found to dominate (not shown). As discussed in section 3e, block-centered compositing of **W** as calculated above yields blocking onset that is physically consistent with previous dynamical descriptions of blocking (e.g., Nakamura et al. 1997; TN01; Paradise et al. 2019). In addition, it is generally true that phase speed tends to zero near the upstream flank of blocked flows (Nakamura and Huang 2018), which would act to suppress the phase propagation term in the complete TN01 formulation. Thus, we take **W**, as defined above, to suffice for the analyses within this paper.

e. Block-centered compositing

To assess any biases in background flow and high-frequency forcing during blocking onset, block-centered compositing is implemented following the methods of Narinesingh et al. (2020). In this work, Z_{500}, Z'_{500}, 250-hPa U (U_{250}), and vertically integrated **W** are composited. Note that U_{250} represents the 30-day low-pass filtered zonal wind field as described in the **W** formulation.

To construct the composites, a given field around the Z'_{500} maximum of each block is collected and projected onto an equal-area grid. This is carried out for the onset phase of each block, defined as the first 2 days the block was recognized by the tracking algorithm. Then, the average over all blocks originating in a given region (Atlantic or Pacific) is computed.
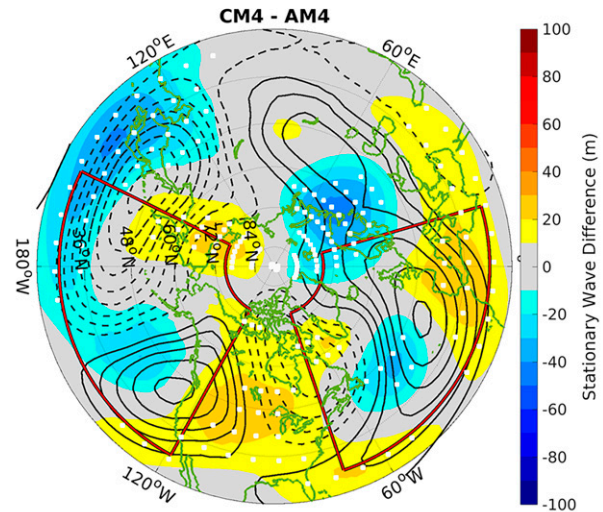
FIG. 4. Z^*_{500} for AM4 (contours) and Z^*_{500} in CM4 minus AM4 (shading). Solid and dashed contours show the positive and negative Z^*_{500}, respectively. The outer contour for the solid (dashed) contours is 25 (-25) m and the contour interval is 25 (-25) m. White stippling denotes regions where Z^*_{500} in the CM4 differs significantly from AM4.

f. Statistical significance testing

To discern statistically significant differences between the GFDL models (AM4 and CM4) and reanalysis (ERA5), the Mann–Whitney U test is employed. One advantage of the U test over other methods such as the t test is that the U test is nonparametric. For each year in each model, the blocking climatology is calculated. Then, for each grid point, U tests are performed between the distributions of the annual blocking frequency in ERA5 and the distributions of annual blocking frequency in AM4 or CM4 at that grid point. The comparison of the distributions gives a robust, nonparametric approach for quantifying the differences in the blocking climatologies. A 95% confidence interval is imposed throughout this paper. The same procedure is followed for the stationary wave and jet analyses.

The block-centered compositing analysis also utilizes the U test. For ERA5, a given field around the centroid of each block in the region of interest is collected and put into a three-dimensional matrix with dimensions longitude by latitude by block number. The same is done for the GFDL models. Then at each corresponding grid point relative to the block centroid, U tests are performed between ERA5 and the GFDL models.

3. Results

a. General circulation features

Tung and Lindzen (1979) suggested that blocking is the product of resonant amplification of stationary waves by transient eddies. Also, stronger stationary waves in idealized models lead to a nonlinear increase in blocking (Paradise et al. 2019; Narinesingh et al. 2020). The zonal wind too plays a key role in
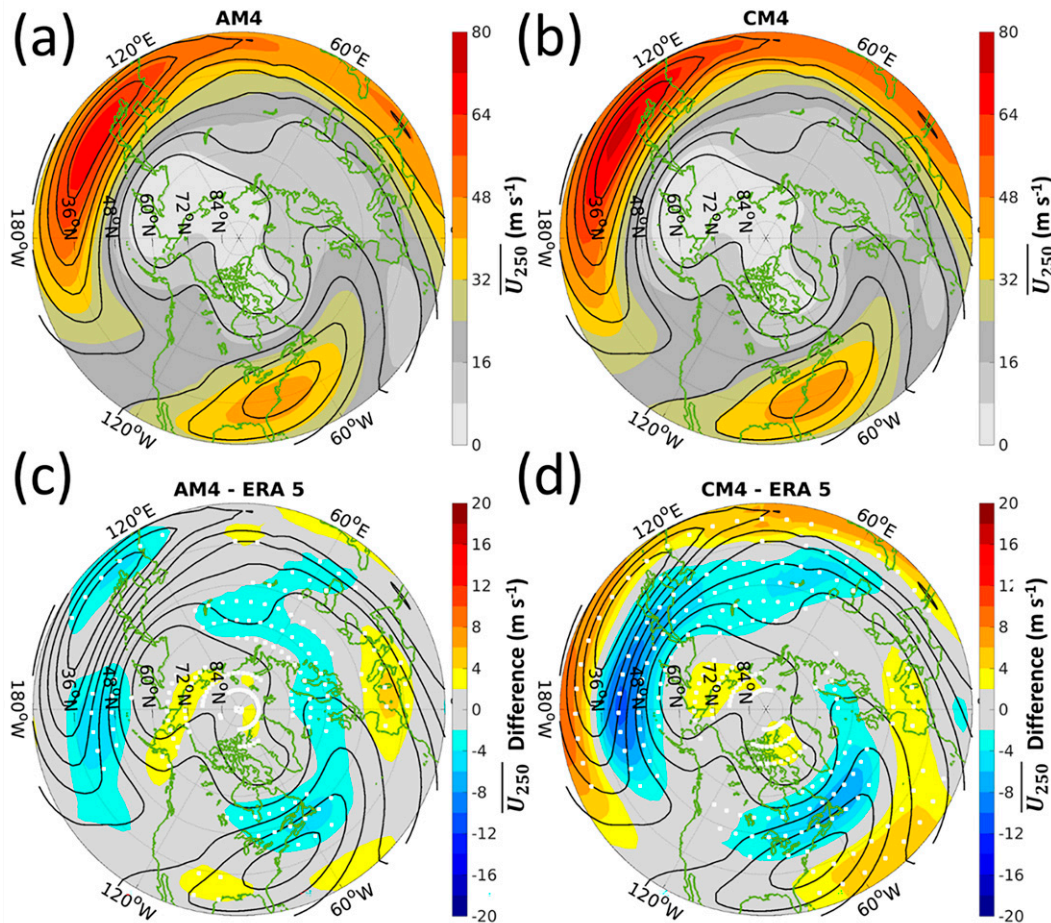
FIG. 5. (top) DJF mean zonal wind at 250 hPa, $\overline{U_{250}}$ for ERA5 (contours) and the GFDL models (shading):
(a) AM4 and (b) CM4. (bottom) $\overline{U_{250}}$ for ERA5 (contours) and $\overline{U_{250}}$ in the GFDL models minus ERA5 (shading):
(c) AM4 and (d) CM4. The outer contour is 8 m s^{-1}, and the contour interval is 8 m s^{-1}. White stippling in (c) and
(d) denotes regions where the $\overline{U_{250}}$ in the GFDL models differs significantly from ERA5.

blocking: on one hand a stronger instantaneous jet carries greater momentum and is thus more difficult to halt, but on the other hand blocking frequency is greater in winter than summer (e.g., Pfahl and Wernli 2012), when the time-mean jet (and baroclinicity) is stronger as compared to summer [explored in idealized models in Hassanzadeh et al. (2014)]. Due to the importance of the stationary wave and upper-tropospheric zonal wind to blocking, we begin by analyzing their representation in the models.

1) STATIONARY WAVE

The stationary wave pattern (Fig. 3) over the northern Pacific basin is generated by the orography and land–sea forcing of Asia and North America, as well as forcing from the tropical Pacific (Held et al. 2002; White et al. 2017; Park and Lee 2021). It features a low pressure, baroclinically rich region in the basin entrance (Chang et al. 2002) that is flanked on its equatorward side by the Pacific upper-level jet maximum (Figs. 3 and 5). On the downstream side of the ocean basin, there is an anticyclonic

stationary wave anomaly forced primarily by the Rocky Mountains and the overall North American topography (Broccoli and Manabe 1992). In the Atlantic basin, an east–west, high–low stationary wave dipole is observed (Fig. 3), similar to the Pacific. This is primarily due to land–sea contrast and topography of both North America and Europe (Seager et al. 2002) and, to a lesser extent, the Gulf Stream (Brayshaw et al. 2009).

AM4 and CM4 produce qualitatively similar stationary wave patterns compared to reanalysis (Figs. 3a,b), although some biases exist (Figs. 3c,d). Near the Atlantic and Pacific blocking maxima (Fig. 2a), both models share similar biases (Figs. 3c,d). In the Pacific, the positive stationary anomaly over the eastern Pacific Ocean is significantly enhanced and biased toward the southwest in both models but decreases over land toward the pole (Figs. 3c,d). For the Atlantic dipole pattern in Z^{*}_{500}, a significant decrease in amplitude is found within the GFDL models (i.e., the low pressure anomaly is not low enough and the high pressure anomaly is not high enough).

Overall, AM4 has less stationary wave biases than CM4 (Figs. 3c,d), which is likely to be partially driven by differences
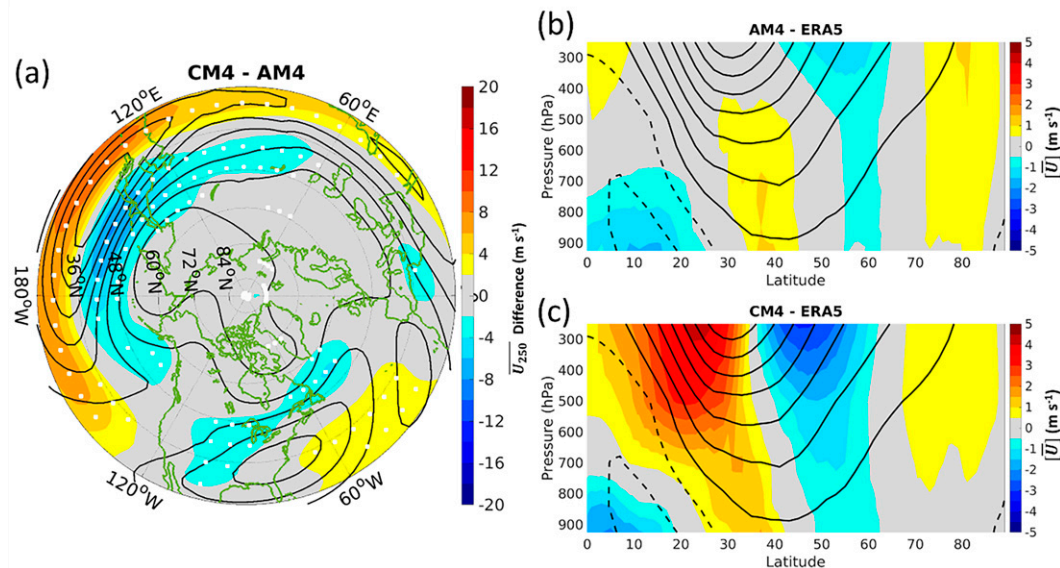
FIG. 6. (a) $\overline{U_{250}}$ for AM4 (contours) and $\overline{U_{250}}$ in CM4 minus AM4 (shading). Contours are drawn every 8 m s^{-1} starting from 8 m s^{-1}. White stippling indicates regions where $\overline{U_{250}}$ in CM4 differs significantly from AM4. (b),(c) DJF zonal-mean zonal wind $[\overline{U}]$ for ERA5 (contours) and DJF zonal-mean zonal wind for (b) AM4 and (c) CM4 minus ERA5 (shading). Solid (dashed) contours in (b) and (c) indicate positive (zero and negative) zonal wind values with outer contour 5 (0) m s^{-1} and contour interval 5 (-5) m s^{-1}.

in SSTs (Fig. 1; Ting and Held 1990; Ting 1991). Both models, however, share similar biases in regions where blocking occurs the most (Figs. 2 and 3). In the Pacific region, AM4 contains root-mean-square (rms) error of 24.8 m whereas CM4 contains an error of 23.4 m. Little significant difference is found between the models in this region (Fig. 4). In the Atlantic region, CM4 contains a higher regional rms error value (20.2 m) compared to AM4 (15.8 m); however, this disagreement is not significant over the whole region. It is driven locally by a more positive stationary wave around northern Africa (Figs. 3 and 4), where blocking occurs only 0%–3% of winter days (Fig. 2).

2) ZONAL BACKGROUND FLOW

Figure 5 shows the time mean zonal wind at 250 hPa ($\overline{U_{250}}$) for the GFDL models. Both models capture two localized jet maxima, one in the Pacific and another, tilted jet maximum in the Atlantic (Figs. 5a–d). For reference, we note that just poleward and downstream of these jet maxima lie the storm tracks, where transient eddy activity maximizes (Hoskins and Hodges 2002; Narinesingh et al. 2020).

Overall, the jet in CM4 has a much larger bias than AM4 (Figs. 5c,d). In the Pacific, the jet maximum is equatorward of that in reanalysis (Fig. 5d), whereas the jet in AM4 has no such bias (Fig. 5c). In the Atlantic, the equatorward bias of the jet maxima in CM4 is greater than AM4 (Fig. 6a). Consistent with this, differences in the zonal mean zonal wind in AM4 are minimal (Fig. 6b), whereas the biases in CM4 indicates a notable equatorward shift in the jet (Fig. 6c).

In a previous version of the GFDL GCM, Delworth et al. (2006) also found an equatorward shift in zonal circulation when comparing a coupled model with an atmosphere-only model.

This shift was associated with an equatorward contraction of the subtropical gyre and Hadley cell, and it contributed to cold biases in SST in the coupled model (Delworth et al. 2006). Clearly, CM4 exhibits a similar contraction of midlatitude circulation compared to AM4, and this has been documented previously (Held et al. 2019). Consistent with this atmospheric circulation change, there is a cold bias in the coupled model SST in both the Atlantic and Pacific (Fig. 1). Held et al. (2019) suggest that the contraction of CM4's midlatitude circulation is a result of tropical cold biases in the upper troposphere, with lesser contribution from extratropical SST biases. The causes of the equatorward shift in CM4's zonal winds pose interesting research questions; however, it is beyond the scope of this work. With relevance to blocking, the main message of this section is that CM4's zonal background flow is equatorward shifted and has a much larger bias compared to AM4.

The forcing of the midlatitude atmosphere by the ocean in the winter is strongly related to meridional SST gradients, especially at the western boundary currents (e.g., Hoskins and Valdes 1990). Therefore, we also analyzed SST gradients for the models (Fig. 7). Over the west Pacific and Atlantic Oceans CM4 has weaker gradients in the midlatitudes compared to AM4. These differences in SST gradients likely contribute to the biases in the zonal wind. But it is interesting to note that the Atlantic SST biases are as large as those in the Pacific, whereas the zonal wind biases are much larger in the Pacific. This supports the suggestions of Held et al. (2019) discussed above, which states that the zonal wind biases are more dependent on tropical forcing biases than midlatitude SST biases. For the purposes of this paper, a key takeaway is this: due to biases in the coupled model, the SST gradients in CM4 are weaker than those in AM4.
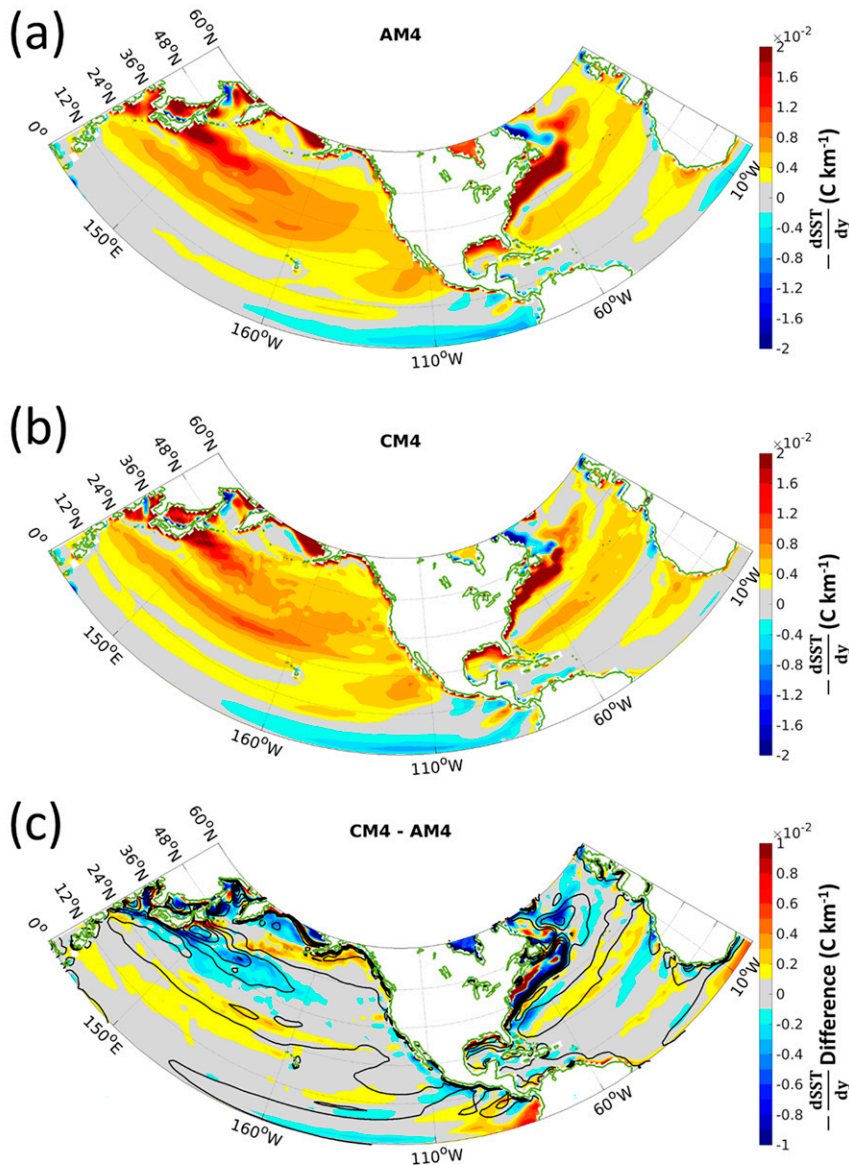
FIG. 7. (a),(b) Negative of the meridional gradient of SST (shading) in (a) AM4 and (b) CM4. (c) Negative meridional gradient of SST in AM4 (contours) and difference between CM4 and AM4 (shading). The outer contour is 0°C km^{-1} and the contour interval is 0.01°C km^{-1}.

b. Blocking climatology

Figure 8 shows the winter blocking climatology for ERA5, AM4, and CM4. Both GFDL models produce a pattern in the blocking climatology that is qualitatively similar to reanalysis (Figs. 8a,b) and consistent with previous findings (Tyrlis and Hoskins 2008; DS13). The blocking climatology features a bimodal pattern with a Pacific maximum just equatorward of the Aleutian Peninsula, and an Atlantic maximum near Greenland that extends into Europe.

Overall, the blocking climatologies of AM4 and CM4 are similar and share various common biases. In both models too much

blocking is generated along the northeastern Pacific coastline (Figs. 8c,d), with significant excess found near the Rocky Mountains. In the Atlantic region, both GFDL models simulate a significant lack of blocking in the Icelandic Basin extending into northern Europe, and an excess of blocking near the Azores high. In line with those biases, the Atlantic blocking maximum is shifted roughly 7.5° south in both GFDL models (Figs. 8c,d).

Figure 9a shows the differences in the blocking climatology between CM4 and AM4. In the Pacific region CM4 produces less blocking than AM4; however, this is not significant and occurs within a region of large interannual blocking variability
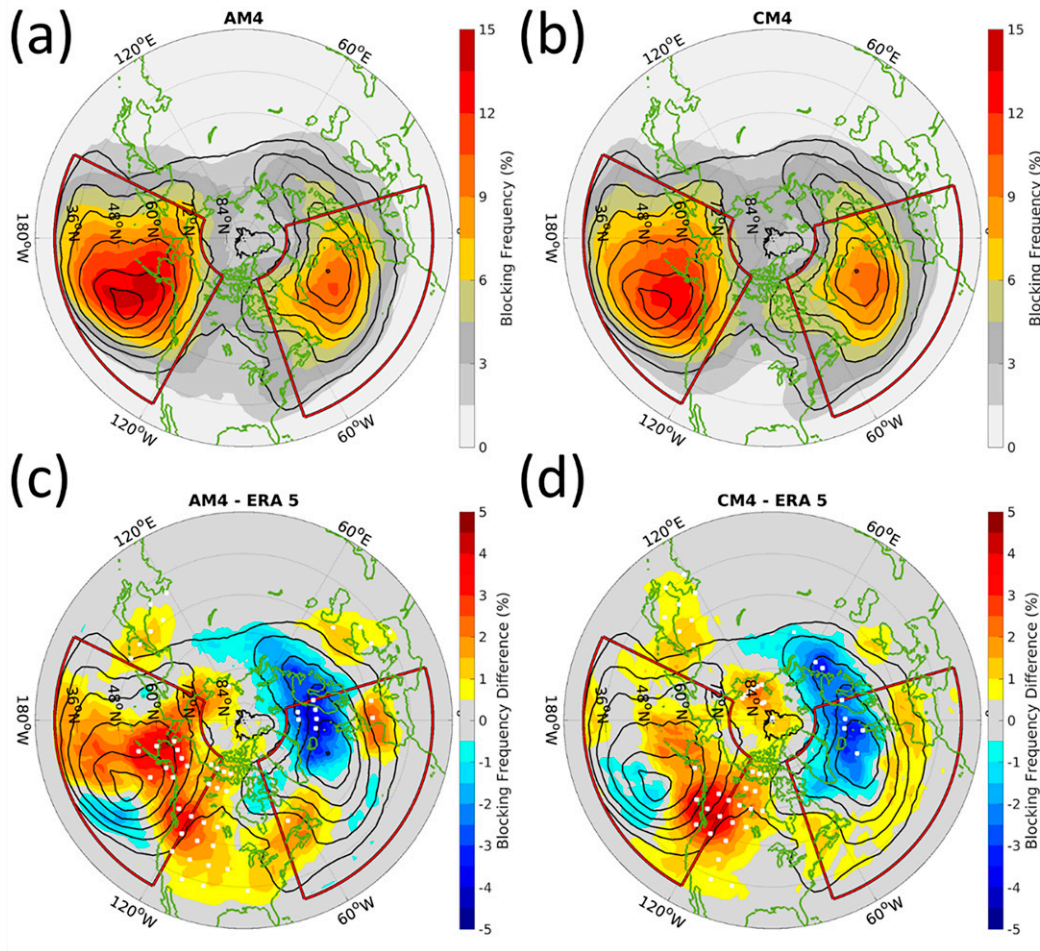
FIG. 8. (top) DJF blocking climatology for ERA5 (contours) and in the GFDL models (shading): (a) AM4 and (b) CM4. (bottom) Blocking climatology for ERA5 (contours) and GFDL models minus ERA5 (shading): (c) AM4 and (d) CM4. White stippling in (c) and (d) denotes regions where the blocking climatology in the GFDL models differs significantly from ERA5. For the ERA5 blocking climatology in all panels, the outer contour and contour interval are 2%.

(Fig. 9b; Tyrlis and Hoskins 2008). In fact, no significant differences are found between the blocking climatologies of AM4 and CM4 in the Pacific and Atlantic regions. In addition, compared to ERA5 both models also exhibit similar biases in interannual variability (not shown).

To quantify regional biases in blocking frequency, for a given region we define the normalized root-mean-square error, F as the following:

$$F = \frac{\sqrt{\frac{1}{A}\sum_{n=1}^{N}\left(f_n - \hat{f}_n\right)^2 a_n}}{\frac{1}{A}\sum_{n=1}^{N}\hat{f}_n a_n}, \qquad (2)$$

where A is total area, N is number of grid points, f_n is the GFDL blocking frequency at a grid point n, $\hat{f}_n$ is the ERA5

blocking frequency, and a_n is area of n. Note that F is essentially a measure of the error in blocking frequency normalized by the area-weighted average of blocking frequency in the region [denominator in Eq. (2)].

Both models show similar amounts of error (Table 1) except in the Pacific region, where CM4 has roughly 25% less error than AM4. This is significant using a U test across all years. Still, the errors found here are similar in terms of relative magnitude, and within a region of high variability (Fig. 9b). The Atlantic and entire midlatitude regions also contain less error in CM4 than AM4, but these differences are not significant. These results were found to be robust to changes $\pm 10°$ in the eastern and western limits, $\pm 5°$ to the northern limit, and $+5°$ to the southern limit of each region. Note that the block tracking algorithm only searches for blocks poleward of 30°.

The relative agreement in error over the entire midlatitudes further emphasizes the similarities in climatological blocking
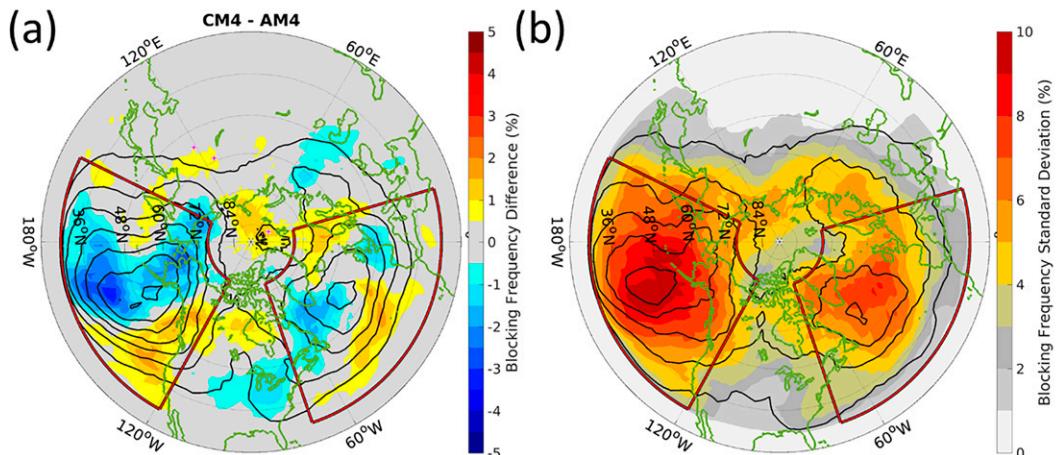
FIG. 9. (a) Blocking climatology for AM4 (contours) and CM4 minus AM4 (shading). Magenta stippling indicates regions where the blocking climatology in CM4 differs significantly from AM4. (b) Standard deviation of the blocking climatology in AM4 (contours) and CM4 (shading). The outer contours and contour interval are both 2% in (a) and (b).

biases between the models, albeit with some compensating errors. This is despite there being major disagreement between the zonal circulation (Figs. 5 and 6) and SST (Fig. 7) in both models. This will be commented on further in the discussion section (section 4).

c. Block count, duration, and area

To gain better insight into the drivers of the blocking frequency biases, we next analyze block event statistics. Table 2 shows the duration and mean number of blocking events per year for the reanalysis and GFDL models by region. In the Pacific region, the GFDL models are in close agreement with ERA5 in terms of number of events per year but simulate an almost 1-day-longer average duration. This difference is not statistically significant, however, due to a large standard deviation in block duration, but the difference is consistent with the enhanced amount of blocking in the Pacific. AM4 and CM4 also produce Pacific blocks whose individual sizes are roughly 0.5 and 0.4 million km^2 larger than those in reanalysis, respectively (Table 3). This difference is not statistically significant because of the large spread in block sizes.

In the Atlantic region, less blocking is simulated in the GFDL models compared to reanalysis (Table 2). A similar number of events per year is found, but the GFDL models have a lower, albeit not significant, average duration of 0.6–0.7 days (Table 2). This decrease in duration agrees with the decrease in blocking frequency (Figs. 8c,d). In terms of area, Atlantic blocks tend to be similar in size across all models and have a smaller average area than Pacific blocks (Table 3).

To summarize, Pacific blocks in the GFDL models are, on average, slightly more persistent and larger than those in reanalysis. Atlantic blocks in the GFDL models are similar in size to reanalysis, but there is a suggestion of shorter average durations. However, we cannot discount the possibility that these differences for the both the Pacific and Atlantic are due to natural variability rather than being a systematic bias. Still, the fact that AM4 and CM4 both exhibit such similar biases in terms of sign and magnitude of the biases in each region adds to the robustness of likeness in blocking biases between the models.

These results for block size and duration are consistent with biases in the blocking climatology (which are statistically significant), showing too much blocking in the Pacific, and too little in the Atlantic. We also note that the block area and duration biases in AM4 and CM4 are another example of

TABLE 1. Normalized RMS error F [Eq. (2)] for regional blocking in AM4 and CM4 compared against ERA5. All regions cover only the midlatitudes (30°–75°N). The Pacific, Atlantic, and all midlatitude regions extend longitudinally over 153.75°E–118.75°W, 71.25°W–16.25°E, and 0°–360°, respectively. The asterisk (*) indicates significant differences between the models.

	Pacific region	Atlantic region	All midlatitudes
AM4	0.29*	0.27	0.34
CM4	0.23	0.23	0.32

TABLE 2. For ERA5 and both GFDL models (AM4 and CM4), block duration (days), standard deviation of block duration (days), and mean number of events per DJF in each region.

	Pacific region	Atlantic region
ERA5	8.3/5.2/3.8	8.5/3.9/1.9
AM4	9.2/6.2/4.1	7.8/3.5/2.2
CM4	9.0/6.0/3.9	7.9/4.9/2.0

TABLE 3. For ERA5 and both GFDL models (AM4 and CM4), mean block area and standard deviation of block area in each region. Both values are in units of 10^6 km^2.

	Pacific region	Atlantic region
ERA5	6.19/1.81	5.45/1.32
AM4	6.69/2.04	5.49/1.79
CM4	6.59/1.86	5.44/1.41

common blocking biases between the models, in addition to biases in the climatology.

d. Zonal background flow during block onset

To assess background flow properties during the onset phase of blocking, compositing analysis of 30-day low-pass filtered zonal wind at 250 hPa (U_{250}) is performed. Figures 10a and 10b show these composites for the Pacific and Atlantic regions, respectively, using ERA5.

Both the Pacific and Atlantic regions feature U_{250} composite maxima upstream and poleward from the blocking center (Figs. 10a,b). There are also minima in composite U_{250}, downstream-equatorward of the block center for both regions. Similar patterns are found when raw 250-hPa zonal wind is composited for 30 days prior to blocking onset (not shown).

In terms of differences between regions, the Pacific Z_{500} composite during the onset phase has a distinct ridge (in fact, it has an omega shape, but to our knowledge there is no automated metric for classifying omega blocks), and U_{250} is stronger (Fig. 10a). In the Atlantic, the diffluent flow pattern is more pronounced (Fig. 10b) and the Z_{500} composite contours exhibit more of an overturning pattern, which is consistent with anticyclonic wavebreaking (e.g., Davini et al. 2012).

AM4 (Figs. 10c,d) and CM4 (Figs. 10e,f) both capture an anticyclonic wavebreaking signature in the Atlantic and ridge behavior in the Pacific. In the Pacific, AM4 exhibits no significant biases, but CM4 has an equatorward shift in composite U_{250} (Fig. 10e) mirroring what was found for the climatological location of the jet (Figs. 5b,d).

The Atlantic blocks feature no significant biases in the upstream and central blocking region for both AM4 and CM4. Downstream-equatorward of the composite block center, however, both models have enhanced zonal flow compared to reanalysis. In addition, AM4 has suppressed zonal flow downstream-poleward of the block center.

e. Transient eddy forcing

Convergence of transient eddy pseudomomentum acts to reinforce blocking by slowing down the westerly flow (Hoskins et al. 1983; Trenberth 1986; Takaya and Nakamura 2001) and replenishing anomalous PV (Shutts 1983; Nakamura and Wallace 1993; Yamazaki and Itoh 2013a). Here, we assess the high-frequency (6-day high-pass-filtered) eddy forcing of blocking in the models using the wave activity flux pseudomomentum, **W**.

Figure 11 shows block-centered composites of Z'_{500}, **W**, and $\nabla \cdot \mathbf{W}$ for Pacific and Atlantic blocks during the onset phase. In ERA5, low pressure minima lie upstream from the

composite block centers (Figs. 11a,b), in agreement with previous findings (Colucci 1985; Nakamura and Wallace 1993). Both regions feature a convergence of **W** on the upstream-equatorward flank of the blocking center.

Both the Pacific (Fig. 11a) and Atlantic (Fig. 11b) high pressure centers are flanked by low pressure minima on their equatorward sides. In the Atlantic, however, the north–south dipole axis is tilted compared to the Pacific region, perhaps related to the southwest-to-northeast orientation in the North Atlantic's climatological circulation. The Atlantic blocks in ERA5 (Fig. 11b) demonstrate stronger **W** convergence compared to those in the Pacific (Fig. 11a). This difference is statistically significant.

The GFDL models (Figs. 11c–f) capture the same patterns of **W** convergence as reanalysis (Figs. 11a,b). There is some suggestion, however, that the Atlantic blocks in AM4 (Fig. 11d) and CM4 (Fig. 11f) demonstrate less forcing, although these differences are not significant throughout the upstream-equatorward convergence area. Both models also reproduce the differences in Atlantic (Figs. 11d,f) and Pacific (Figs. 11c,e) blocking in terms of high–low dipole orientation.

One aspect the models fail to reproduce is the differences in magnitude of **W** convergence between the Atlantic and Pacific regions. Aside from this, however, the results of this subsection suggest that the GFDL models properly represent the onset phases of both Pacific and Atlantic blocking in terms of transient eddy forcing and geopotential height evolution.

4. Discussion

Using an idealized traffic-jam model, Paradise et al. (2019) and others found blocking occurrence responds to changes in the stationary wave (Tung and Lindzen 1979; Luo 2005), jet (Barnes and Hartmann 2010; de Vries et al. 2013), and eddy forcing (Shutts 1983; Yamazaki and Itoh 2013b). As such, here we discuss consistencies and inconsistencies in the GFDL models regarding blocking and the aforementioned circulation features. As a reminder, we note that the jet and stationary wave analysis discussed throughout this paper were found to be insensitive to the removal or inclusion of the time steps with blocks.

The models generate too much blocking in the Pacific region and too little blocking in the Atlantic (Fig. 8). In both models, this result is consistent with the enhanced positive stationary wave anomaly found in the Pacific and weakened stationary wave in the Atlantic (Fig. 3). This also agrees with Paradise et al. (2019), who found a positive relationship between blocking and stationary wave amplitude.

The Pacific and Atlantic blocking biases shared by AM4 and CM4 are also in agreement with theory and other previous results regarding stationary waves. In the wave activity traffic jam theory of blocking developed by Nakamura and Huang (2018), an enhanced stationary wave results in a region's decreased capacity for wave activity fluxes, thus leading to blocking. Furthermore, Narinesingh et al. (2020) also found increases in blocking when an idealized moist GCM was configured into a strong stationary wave regime
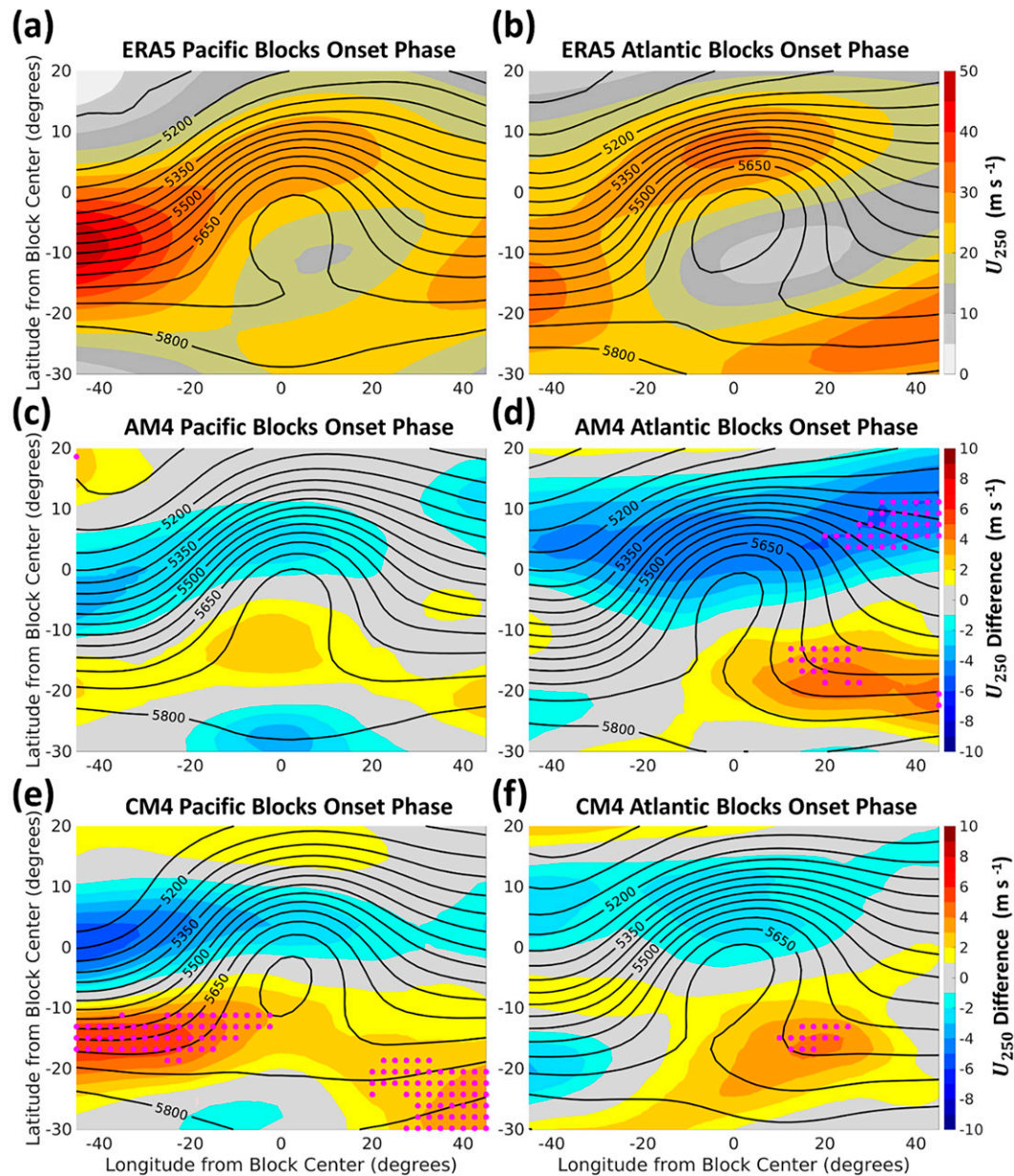
FIG. 10. (top) For the block onset phase, block-centered composites of unfiltered 500-hPa geopotential height (m; contours) and 30-day low-pass-filtered 250 hPa zonal wind U_{250} (shading) for (a) Pacific and (b) Atlantic blocks in ERA5. (middle),(bottom) For the block onset phase, block-centered composites of unfiltered 500-hPa geopotential height (contours) and difference between block-center composited U_{250} in the GFDL models and ERA5 (shading): (middle) computed using AM4 for (c) Pacific and (d) Atlantic blocks and (e),(f) computed using CM4 for (e) Pacific and (f) Atlantic blocks. Magenta stippling in (c)–(f) indicate significant differences between the corresponding GFDL model and ERA5.

compared to zonally symmetric and weaker stationary wave integrations.

The relationship between the blocking climatology and the zonal wind in AM4 and CM4 is not so clear, however. Despite CM4 containing an equatorward shifted zonal flow compared to AM4 (Fig. 6), the models exhibit similar biases in terms of their blocking climatologies (Fig. 8). Barnes and Hartmann (2010) found that higher blocking frequencies corresponded to

equatorward jets in CMIP models. Their result agrees with the Pacific overgeneration of blocks in CM4 but disagrees with CM4 and AM4's Atlantic blocking deficiencies.

CM4's Pacific blocks also contain enhanced zonal background flow on the upstream-equatorward flank of the blocking high (Fig. 10e), near the meridional high–low dipole (Fig. 11e). This is inconsistent with the findings of Paradise et al. (2019), who found decreased blocking in stronger zonal flows. In the Atlantic, the
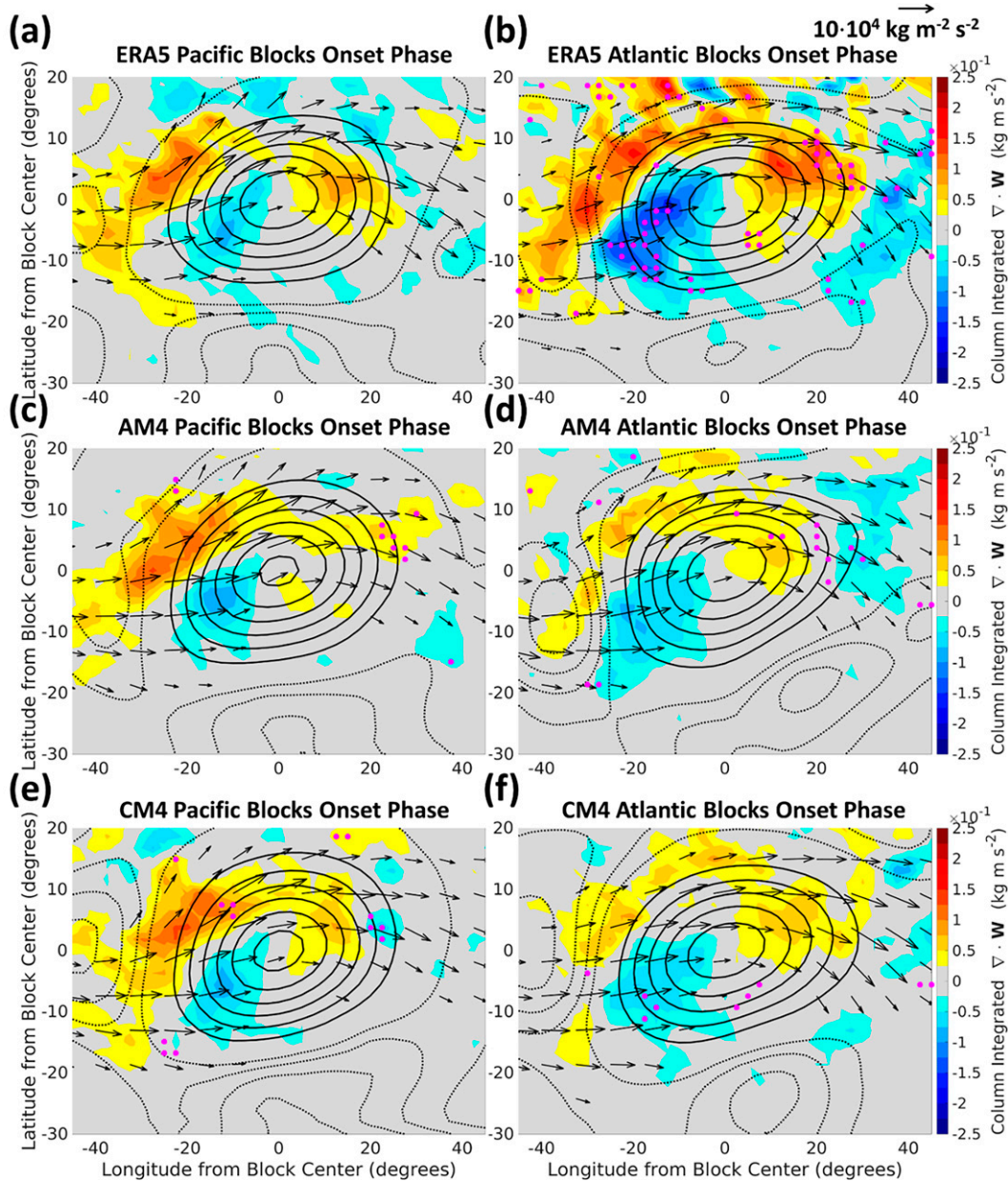
FIG. 11. (a),(c),(e) For the onset phase of Pacific blocking events, block-centered composites of positive 500-hPa geopotential height anomalies (solid contours), negative 500-hPa geopotential height anomalies (dashed contours), column-integrated wave activity flux **W** (arrows), and $\nabla \cdot \mathbf{W}$ (shading) for (a) ERA5, (c) AM4, and (e) CM4. (b),(d),(f) As in (a), (c), and (e), but for Atlantic blocks. Positive (negative) geopotential height contours have an outer contour of 50 (−20) m and a contour interval of 50 (−20) m. **W** is calculated using 6-day high-pass-filtered fields. Vectors with magnitudes less than 5×10^4 kg m^{-2} s^{-2} are masked. Magenta stippling indicates significant differences in $\nabla \cdot \mathbf{W}$ between (b) ERA5's Pacific and Atlantic blocks, and (c)–(f) the corresponding GFDL model and ERA5.

decrease in blocking near Iceland is also not expected given the weakened background flow (Fig. 5). In terms of transient eddy forcing during the onset phase of blocking, the GFDL models show little difference from reanalysis (Fig. 11). This is despite various jet biases between the models. Yamazaki and Itoh (2013b) also found results consistent to ours, where transient eddy forcing of blocks was found to be insensitive to jet strength and placement.

Taken together, these results regarding the zonal winds suggest the model biases in blocking may come from any of the following:

1) mean-state biases in the stationary wave or physics that is not fully captured by the models,

2) blocks in the Pacific and Atlantic having substantial differences in their interaction with the background flow, or
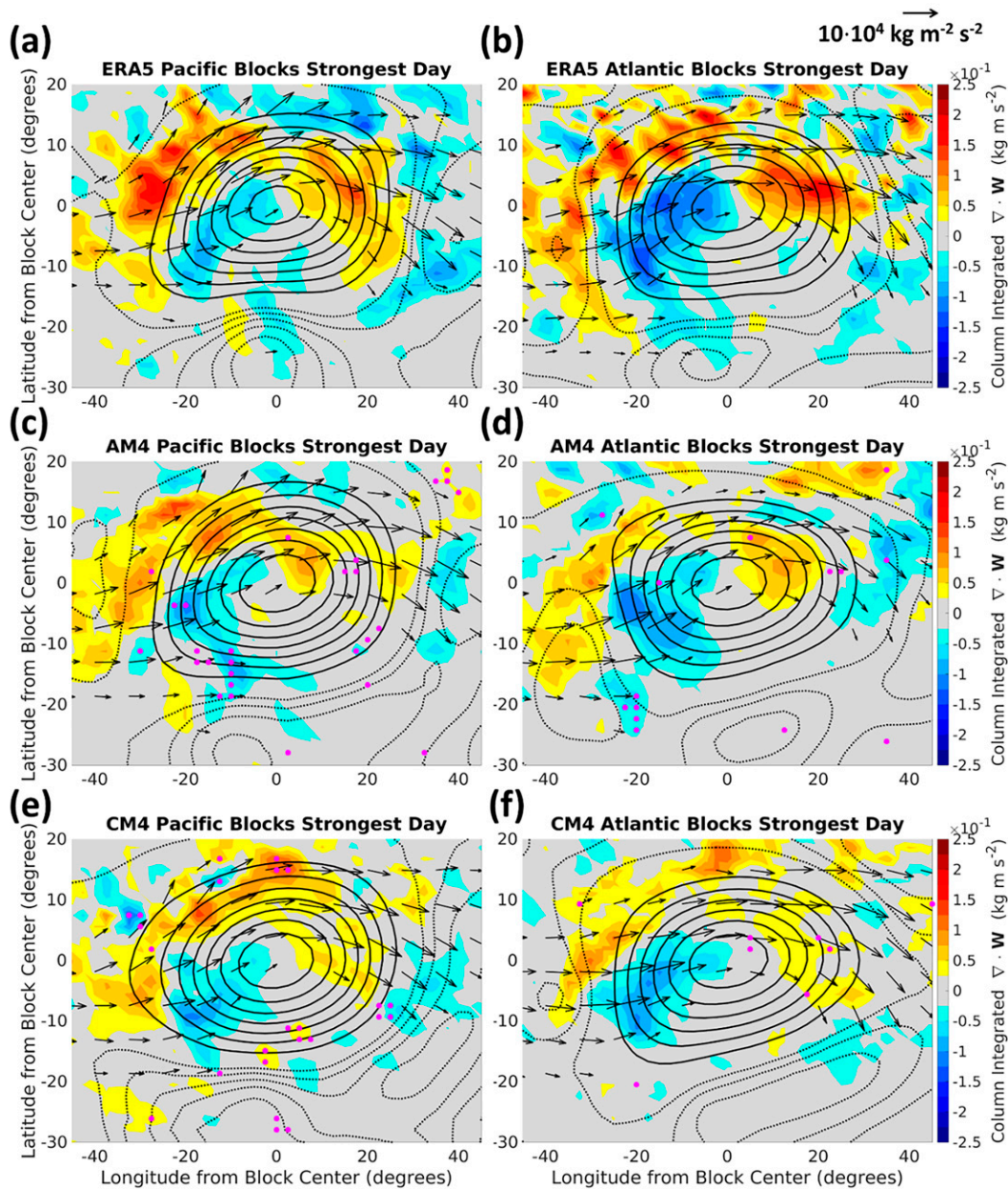
FIG. 12. (a),(c),(e) For the strongest days of Pacific blocking events, block-centered composites of positive 500-hPa geopotential height anomalies (solid contours), negative 500-hPa geopotential height anomalies (dashed contours), column-integrated wave activity flux **W** (arrows), and $\nabla \cdot \mathbf{W}$ (shading) for (a) ERA5, (c) AM4, and (e) CM4. (b),(d),(f) As in (a), (c), and (e), but for Atlantic blocks. Positive (negative) geopotential height contours have an outer contour of 50 (-20) m and a contour interval of 50 (-20) m. **W** is calculated using 6-day high-pass-filtered fields. Vectors with magnitudes less than 5×10^4 kg m^{-2} s^{-1} are masked. Magenta stippling in (c)–(f) indicates significant differences in $\nabla \cdot \mathbf{W}$ between the corresponding GFDL model and ERA5.

3) aspects of blocking onset and maintenance that have not yet been considered.

Maintenance of blocking is also critical to blocking longevity (Shutts 1983; Pfahl et al. 2015). Figure 12 shows block centered composites of $\nabla \cdot \mathbf{W}$ during the strongest days of blocks as defined

by the maximum Z'_{500} field over block life cycles. Here we only consider blocks that remain in their region of origin based on the duration criteria described in the methods section (section 2c). Across models, on average the strongest block days occur between days 3.5–4 in the Atlantic and days 5–5.5 in the Pacific.

Little difference is found between the GFDL models and ERA5 during the strongest days, except there is some suggestion that AM4's Pacific **W** convergence is greater (Fig. 12c). This could indicate enhanced transient eddy forcing, consistent with the overgeneration of blocking in the region. However, a similar difference is not found in CM4.

Herein we focus on the transient eddy maintenance of blocking through wave-activity fluxes, but other studies have found latent heating (Pfahl et al. 2015) to play a prominent role as well. Thus, a more comprehensive look at the dynamic and thermodynamic maintenance of blocking throughout their life cycle is warranted in future study.

Overall, stationary wave biases remain the most consistent with blocking biases for the GFDL models, but the work here cannot attribute causality without more rigorous testing of the models. In future work, we plan on investigating the response of blocking to changes in the stationary wave and jet as well as dynamic and thermodynamic maintenance mechanisms. We note that such a study would need to consider the coupling between the general circulation features themselves, as well as block maintenance mechanisms.

5. Summary and conclusions

GFDL's atmosphere only (AM4) and coupled atmosphere–ocean (CM4) general circulation models reproduce the overall spatial pattern of the blocking climatology (Fig. 8) with a similar number of events per DJF season (Table 2). In the Pacific, however, the modeled blocking frequency is biased high compared to reanalysis. This could be due to each model's tendency to generate blocks that are spatially too large and last too long, although the large variability in block duration and area makes it difficult to conclusively say so.

In the Atlantic region, AM4 and CM4 both have less blocking than reanalysis. Here, the distribution of spatial size of individual blocks is similar to reanalysis, but there is a suggestion that they are slightly less persistent, albeit with high uncertainty.

Blocking onset dynamics is also assessed within the models. In terms of the 500-hPa geopotential height field, both models produce differences between Pacific and Atlantic blocking that match with observations (Fig. 10). In the Pacific, the Z_{500} field features an amplified ridge during blocking onset, whereas in the Atlantic a signature of anticyclonic wavebreaking is found.

The background zonal flow during block onset is generally captured within the models (Fig. 10), except CM4 features an equatorward shift for Pacific blocks. In terms of high-frequency eddy forcing during blocking onset, both models produce similar patterns in wave activity flux convergence compared to reanalysis (Fig. 11). The models do not, however, produce the stronger convergence found for Atlantic blocking compared to Pacific.

Our analysis of general circulation features previously shown to influence blocking revealed a mixture of results. First, both models capture the overall spatial pattern of the stationary wave (Z_{500}^*; Fig. 3), but some biases exist. In the Pacific region, AM4 and CM4 produce an enhanced positive stationary wave anomaly. In the Atlantic, the amplitude of the stationary wave is too small in both models (Fig. 3). These biases match in location and sign with the biases in blocking, and the biases are present even if only the time steps without blocking are considered.

For the zonal wind, there were differences between the models that did not align with differences in blocking. CM4 features an equatorward bias in the Pacific jet location ($\overline{U_{250}}$; Fig. 5) that is not found in AM4 (Fig. 5). The southwest-to-northeast tilt of the Atlantic jet is captured by AM4 and CM4, but the jet maximum is biased equatorward in both models. The Atlantic shifting is more extreme in CM4 than AM4 (Fig. 6a). CM4's equatorward shifted zonal flow is consistent with contracted Hadley circulation (Figs. 6b,c). This is also accompanied by generally colder SSTs in CM4 compared to AM4 (Fig. 1).

Despite large differences in the jet and SSTs between AM4 and CM4, the two models produce similar blocking climatologies (Fig. 8). Overall, the commonalities in blocking climatology, duration, and area biases in AM4 and CM4 suggest a weak sensitivity to the difference in zonal flow (Fig. 6) and ocean forcing (Fig. 7) between the models—or some compensating biases. At the same time, both models exhibit similar stationary wave and blocking climatology biases, and few transient eddy forcing biases (Figs. 11 and 12). This could suggest that the stationary wave could play the more prevalent role in driving the models' biases in blocking. Further study is planned to test this hypothesis.

REFERENCES

Adcroft, A., and Coauthors, 2019: The GFDL Global Ocean and Sea Ice Model OM4.0: Model description and simulation features. *J. Adv. Model. Earth Syst.*, **11**, 3167–3211, https://doi.org/10.1029/2019MS001726.

Anstey, J. A., and Coauthors, 2013: Multi-model analysis of Northern Hemisphere winter blocking: Model biases and the role of resolution. *J. Geophys. Res. Atmos.*, **118**, 3956–3971, https://doi.org/10.1002/jgrd.50231.

Barnes, E. A., and D. L. Hartmann, 2010: Influence of eddy-driven jet latitude on North Atlantic jet persistence and blocking frequency in CMIP3 integrations. *Geophys. Res. Lett.*, **37**, L23802, https://doi.org/10.1029/2010GL045700.

——, J. Slingo, and T. Woollings, 2012: A methodology for the comparison of blocking climatologies across indices, models and climate scenarios. *Climate Dyn.*, **38**, 2467–2481, https://doi.org/10.1007/s00382-011-1243-6.

Berrisford, P., B. J. Hoskins, and E. Tyrlis, 2007: Blocking and Rossby wave breaking on the dynamical tropopause in the Southern Hemisphere. *J. Atmos. Sci.*, **64**, 2881–2898, https://doi.org/10.1175/JAS3984.1.

Booth, J. F., E. Dunn-Sigouin, and S. Pfahl, 2017: The relationship between extratropical cyclone steering and blocking along the North American east coast. *Geophys. Res. Lett.*, **44**, 11976–11984, https://doi.org/10.1002/2017GL075941.

——, V. Narinesingh, K. L. Towey, and J. Jeyaratnam, 2021: Storm surge, blocking, and cyclones: A compound hazards analysis for the northeast United States. *J. Appl. Meteor. Climatol.*, **60**, 1531–1544, https://doi.org/10.1175/JAMC-D-21-0062.1.

Brayshaw, D. J., B. Hoskins, and M. Blackburn, 2009: The basic ingredients of the North Atlantic storm track. Part I: Land–sea contrast and orography. *J. Atmos. Sci.*, **66**, 2539–2558, https://doi.org/10.1175/2009JAS3078.1.

Broccoli, A. J., and S. Manabe, 1992: The effects of orography on midlatitude Northern Hemisphere dry climates. *J. Climate*, **5**, 1181–1201, https://doi.org/10.1175/1520-0442(1992)005<1181:TEOOOM>2.0.CO;2.

Chang, E. K. M., S. Lee, and K. L. Swanson, 2002: Storm track dynamics. *J. Climate*, **15**, 2163–2183, https://doi.org/10.1175/1520-0442(2002)015<02163:STD>2.0.CO;2.

Colucci, S. J., 1985: Explosive cyclogenesis and large-scale circulation changes: Implications for atmospheric blocking. *J. Atmos. Sci.*, **42**, 2701–2717, https://doi.org/10.1175/1520-0469(1985)042<2701:ECALSC>2.0.CO;2.

D'Andrea, F., and Coauthors, 1998: Northern Hemisphere atmospheric blocking as simulated by 15 atmospheric general circulation models in the period 1979–1988. *Climate Dyn.*, **14**, 385–407, https://doi.org/10.1007/s003820050230.

Davini, P., and F. D'Andrea, 2016: Northern Hemisphere atmospheric blocking representation in global climate models. *J. Climate*, **29**, 8823–8840, https://doi.org/10.1175/JCLI-D-16-0242.1.

——, and ——, 2020: From CMIP3 to CMIP6: Northern Hemisphere atmospheric blocking simulation in present and future climate. *J. Climate*, **33**, 10021–10038, https://doi.org/10.1175/JCLI-D-19-0862.1.

——, C. Cagnazzo, S. Gualdi, and A. Navarra, 2012: Bidimensional diagnostics, variability, and trends of Northern Hemisphere blocking. *J. Climate*, **25**, 6496–6509, https://doi.org/10.1175/JCLI-D-12-00032.1.

——, S. Corti, F. D'Andrea, G. Rivière, and J. von Hardenberg, 2017: Improved winter European atmospheric blocking frequencies in high-resolution global climate simulations. *J. Adv. Model. Earth Syst.*, **9**, 2615–2634, https://doi.org/10.1002/2017MS001082.

Delworth, T. L., and Coauthors, 2006: GFDL's CM2 global coupled climate models. Part I. *J. Climate*, **19**, 643–674, https://doi.org/10.1175/JCLI3629.1.

de Vries, H., T. Woollings, J. Anstey, R. Haarsma, and W. Hazeleger, 2013: Atmospheric blocking and its relation to jet changes in a future climate. *Climate Dyn.*, **41**, 2643–2654, https://doi.org/10.1007/s00382-013-1699-7.

Dunn-Sigouin, E., and S. Son, 2013: Northern Hemisphere blocking frequency and duration in the CMIP5 models. *J. Geophys. Res. Atmos.*, **118**, 1179–1188, https://doi.org/10.1002/jgrd.50143.

Hartmann, D. L., and S. J. Ghan, 1980: A statistical study of the dynamics of blocking. *Mon. Wea. Rev.*, **108**, 1144–1159, https://doi.org/10.1175/1520-0493(1980)108<1144:ASSOTD>2.0.CO;2.

Hassanzadeh, P., Z. Kuang, and B. F. Farrell, 2014: Responses of midlatitude blocks and wave amplitude to changes in the meridional temperature gradient in an idealized dry GCM. *Geophys. Res. Lett.*, **41**, 5223–5232, https://doi.org/10.1002/2014GL060764.

Held, I. M., M. Ting, and H. Wang, 2002: Northern winter stationary waves. *J. Climate*, **15**, 2125–2144, https://doi.org/10.1175/1520-0442(2002)015<2125:NWSWTA>2.0.CO;2.

——, and Coauthors, 2019: Structure and performance of GFDL's CM4.0 climate model. *J. Adv. Model. Earth Syst.*, **11**, 3691–3727, https://doi.org/10.1029/2019MS001829.

Hersbach, H., and Coauthors, 2020: The ERA5 global reanalysis. *Quart. J. Roy. Meteor. Soc.*, **146**, 1999–2049, https://doi.org/10.1002/qj.3803.

Hoskins, B. J., and P. J. Valdes, 1990: On the existence of storm-tracks. *J. Atmos. Sci.*, **47**, 1854–1864, https://doi.org/10.1175/1520-0469(1990)047<1854:OTEOST>2.0.CO;2.

——, and K. I. Hodges, 2002: New perspectives on the Northern Hemisphere winter storm tracks. *J. Atmos. Sci.*, **59**, 1041–1061, https://doi.org/10.1175/1520-0469(2002)059<1041:NPOTNH>2.0.CO;2.

——, G. H. White, and I. N. James, 1983: The shape, propagation and mean-flow interaction of large-scale weather systems. *J. Atmos. Sci.*, **40**, 1595–1612, https://doi.org/10.1175/1520-0469(1983)040<1595:TSPAMF>2.0.CO;2.

Jiang, T., K. Evans, M. Branstetter, P. Caldwell, R. Neale, P. J. Rasch, Q. Tang, and S. Xie, 2019: Northern Hemisphere blocking in ~25-km-resolution E3SM v0.3 atmosphere–land simulations. *J. Geophys. Res. Atmos.*, **124**, 2465–2482, https://doi.org/10.1029/2018JD028892.

Jung, T., and Coauthors, 2012: High-resolution global climate simulations with the ECMWF model in Project Athena: Experimental design, model climate, and seasonal forecast skill. *J. Climate*, **25**, 3155–3172, https://doi.org/10.1175/JCLI-D-11-00265.1.

Kleiner, N., P. W. Chan, L. Wang, D. Ma, and Z. Kuang, 2021: Effects of climate model mean-state bias on blocking underestimation. *Geophys. Res. Lett.*, **48**, e2021GL094129, https://doi.org/10.1029/2021GL094129.

Luo, D., 2005: A barotropic envelope Rossby soliton model for block–eddy interaction. Part I: Effect of topography. *J. Atmos. Sci.*, **62**, 5–21, https://doi.org/10.1175/1186.1.

Lupo, A. R., 2020: Atmospheric blocking events: A review. *Ann. N. Y. Acad. Sci.*, **1504**, 5–24, https://doi.org/10.1111/nyas.14557.

Masato, G., B. J. Hoskins, and T. J. Woollings, 2013: Winter and summer Northern Hemisphere blocking in CMIP5 models. *J. Climate*, **26**, 7044–7059, https://doi.org/10.1175/JCLI-D-12-00466.1.

Matsueda, M., R. Mizuta, and S. Kusunoki, 2009: Future change in wintertime atmospheric blocking simulated using a 20-km-mesh atmospheric global circulation model. *J. Geophys. Res. Atmos.*, **114**, D12114, https://doi.org/10.1029/2009JD011919.

Mattingly, K. S., J. T. McLeod, J. A. Knox, J. M. Shepherd, and T. L. Mote, 2015: A climatological assessment of Greenland blocking conditions associated with the track of Hurricane Sandy and historical North Atlantic hurricanes. *Int. J. Climatol.*, **35**, 746–760, https://doi.org/10.1002/joc.4018.

Nakamura, H., and J. M. Wallace, 1993: Synoptic behavior of baroclinic eddies during the blocking onset. *Mon. Wea. Rev.*, **121**, 1892–1903, https://doi.org/10.1175/1520-0493(1993)121<1892:SBOBED>2.0.CO;2.

——, M. Nakamura, and J. L. Anderson, 1997: The role of high- and low-frequency dynamics in blocking formation. *Mon. Wea. Rev.*, **125**, 2074–2093, https://doi.org/10.1175/1520-0493(1997)125<2074:TROHAL>2.0.CO;2.

Nakamura, N., and C. S. Y. Huang, 2018: Atmospheric blocking as a traffic jam in the jet stream. *Science*, **361**, 42–47, https://doi.org/10.1126/science.aat0721.

Narinesingh, V., J. F. Booth, S. K. Clark, and Y. Ming, 2020: Atmospheric blocking in an aquaplanet and the impact of orography. *Wea. Climate Dyn.*, **1**, 293–311, https://doi.org/10.5194/wcd-1-293-2020.

Paradise, A., C. B. Rocha, P. Barpanda, and N. Nakamura, 2019: Blocking statistics in a varying climate: Lessons from a "traffic jam" model with pseudostochastic forcing. *J. Atmos. Sci.*, **76**, 3013–3027, https://doi.org/10.1175/JAS-D-19-0095.1.

Park, M., and S. Lee, 2021: Is the stationary wave bias in CMIP5 simulations driven by latent heating biases? *Geophys. Res. Lett.*, **48**, e2020GL091678, https://doi.org/10.1029/2020GL091678.

Pfahl, S., and H. Wernli, 2012: Quantifying the relevance of atmospheric blocking for co-located temperature extremes in the Northern Hemisphere on (sub-)daily time scales. *Geophys. Res. Lett.*, **39**, L12807, https://doi.org/10.1029/2012GL052261.

——, C. Schwierz, M. Croci-Maspoli, C. M. Grams, and H. Wernli, 2015: Importance of latent heat release in ascending air streams for atmospheric blocking. *Nat. Geosci.*, **8**, 610–614, https://doi.org/10.1038/ngeo2487.

Rex, D. F., 1950: Blocking action in the middle troposphere and its effect upon regional climate. *Tellus*, **2**, 196–211, https://doi.org/10.1111/j.2153-3490.1950.tb00331.x.

Scaife, A. A., D. Copsey, C. Gordon, C. Harris, T. Hinton, S. Keeley, A. O'Neill, M. Roberts, and K. Williams, 2011: Improved Atlantic winter blocking in a climate model. *Geophys. Res. Lett.*, **38**, L23703, https://doi.org/10.1029/2011GL049573.

Schiemann, R., and Coauthors, 2020: Northern Hemisphere blocking simulation in current climate models: Evaluating progress from the Climate Model Intercomparison Project Phase 5 to 6 and sensitivity to resolution. *Wea. Climate Dyn.*, **1**, 277–292, https://doi.org/10.5194/wcd-1-277-2020.

Seager, R., D. S. Battisti, J. Yin, N. Gordon, N. Naik, A. C. Clement, and M. A. Cane, 2002: Is the Gulf Stream responsible for Europe's mild winters? *Quart. J. Roy. Meteor. Soc.*, **128**, 2563–2586, https://doi.org/10.1256/qj.01.128.

Shutts, G. J., 1983: The propagation of eddies in diffluent jetstreams: Eddy vorticity forcing of 'blocking' flow fields. *Quart. J. Roy. Meteor. Soc.*, **109**, 737–761.

Sillmann, J., M. Croci-Maspoli, M. Kallache, and R. W. Katz, 2011: Extreme cold winter temperatures in Europe under the influence of North Atlantic atmospheric blocking. *J. Climate*, **24**, 5899–5913, https://doi.org/10.1175/2011JCLI4075.1.

Steinfeld, D., M. Boettcher, R. Forbes, and S. Pfahl, 2020: The sensitivity of atmospheric blocking to upstream latent heating—Numerical experiments. *Wea. Climate Dyn.*, **1**, 405–426, https://doi.org/10.5194/wcd-1-405-2020.

Takaya, K., and H. Nakamura, 2001: A formulation of a phase-independent wave-activity flux for stationary and migratory quasigeostrophic eddies on a zonally varying basic flow. *J. Atmos. Sci.*, **58**, 608–627, https://doi.org/10.1175/1520-0469(2001)058<0608:AFOAPI>2.0.CO;2.

Ting, M., 1991: The stationary wave response to a midlatitude SST anomaly in an idealized GCM. *J. Atmos. Sci.*, **48**, 1249–1275, https://doi.org/10.1175/1520-0469(1991)048<1249:TSWRTA>2.0.CO;2.

——, and I. M. Held, 1990: The stationary wave response to a tropical SST anomaly in an idealized GCM. *J. Atmos. Sci.*, **47**, 2546–2566, https://doi.org/10.1175/1520-0469(1990)047<2546:TSWRTA>2.0.CO;2.

Trenberth, K. E., 1986: An assessment of the impact of transient eddies on the zonal flow during a blocking episode using localized Eliassen-Palm flux diagnostics. *J. Atmos. Sci.*, **43**, 2070–2087, https://doi.org/10.1175/1520-0469(1986)043<2070:AAOTIO>2.0.CO;2.

Tung, K.-K., and R. S. Lindzen, 1979: A theory of stationary long waves. Part I: A simple theory of blocking. *Mon. Wea. Rev.*, **107**, 714–734, https://doi.org/10.1175/1520-0493(1979)107<0714:ATOSLW>2.0.CO;2.

Tyrlis, E., and B. J. Hoskins, 2008: Aspects of a Northern Hemisphere atmospheric blocking climatology. *J. Atmos. Sci.*, **65**, 1638–1652, https://doi.org/10.1175/2007JAS2337.1.

Wang, L., and Z. Kuang, 2019: Evidence against a general positive eddy feedback in atmospheric blocking. 17 pp., https://doi.org/10.31223/OSF.IO/KMGQV.

White, R. H., D. S. Battisti, and G. H. Roe, 2017: Mongolian mountains matter most. *J. Climate*, **30**, 4065–4082, https://doi.org/10.1175/JCLI-D-16-0401.1.

Wolf, G., and V. Wirth, 2017: Diagnosing the horizontal propagation of Rossby wave packets along the midlatitude waveguide. *Mon. Wea. Rev.*, **145**, 3247–3264, https://doi.org/10.1175/MWR-D-16-0355.1.

Woollings, T., and Coauthors, 2018: Blocking and its response to climate change. *Curr. Climate Change Rep.*, **4**, 287–300, https://doi.org/10.1007/s40641-018-0108-z.

Yamazaki, A., and H. Itoh, 2013a: Vortex–vortex interactions for the maintenance of blocking. Part I: The selective absorption mechanism and a case study. *J. Atmos. Sci.*, **70**, 725–742, https://doi.org/10.1175/JAS-D-11-0295.1.

——, and ——, 2013b: Vortex–vortex interactions for the maintenance of blocking. Part II: Numerical experiments. *J. Atmos. Sci.*, **70**, 743–766, https://doi.org/10.1175/JAS-D-12-0132.1.

——, M. Honda, and A. Kuwano-Yoshida, 2015: Heavy snowfall in Kanto and on the Pacific Ocean side of northern Japan associated with western Pacific blocking. *SOLA*, **11**, 59–64, https://doi.org/10.2151/sola.2015-013.

Yeh, T., 1949: On energy dispersion in the atmosphere. *J. Meteor.*, **6** (1), 1–16, https://doi.org/10.1175/1520-0469(1949)006<0001:OEDITA>2.0.CO;2.

Zhao, M., 2018: The GFDL Global Atmosphere and Land Model AM4.0/LM4.0: 1. Simulation characteristics with prescribed SSTs. *J. Adv. Model. Earth Syst.*, **10**, 691–734, https://doi.org/10.1002/2017MS001208.